EUROPEAN ORGANIZATION FOR NUCLEAR RESEARCH
European Laboratory for Particle Physics

Large Hadron Collider Project

LHC Project Report 1083

A DEMONSTRATION EXPERIMENT FOR THE MAIN FIELD TRACKING AND THE SEXTUPOLE AND DECAPOLE COMPENSATION IN THE LHC MAIN MAGNETS

P. Xydi[1], N. Sammut[1], R. Alemany Fernandez[2], L. Bottura[1], G. Deferne[1], M. Lamont[2], J. Miles[1], R. Mompo[1], M. Strzelczyk[2], W. Venturini Delsolaro[2]

Abstract

A dedicated measurement campaign was set up to test the FiDeL concept and its LSA implementation. The test was performed by demonstrating the tracking of B_1 and B_2 for two LHC main dipoles and one LHC main quadrupole. It also included the compensation of the b_3 and b_5 harmonics in the dipole magnets using the sextupole and decapole corrector magnets.

In this report we present the techniques developed to power the magnets for these tests during the current ramps; the instrumentation and data acquisition setup used to perform the tracking experiments; the calibration procedure and data corrections employed; and finally the main results obtained.

LHC-PROJECT-REPORT-1083

1 CERN, Accelerator Technology Department, Geneva, Switzerland
2 CERN, Accelerators & Beams Department, Geneva, Switzerland

CERN
CH - 1211 Geneva 23
Switzerland

Geneva, 18/06/2008

1. INTRODUCTION

The LHC has unprecedented demands on the control of the field and field errors during injection, acceleration, squeeze and collision. One of the most stringent requirements during the energy ramp of the Large Hadron Collider (LHC) at CERN is to have a constant ratio between dipole-quadrupole and dipole-dipole field so as to control the variation of the betatron tune and ensure that the beam orbit remains the same throughout the acceleration phase, hence avoiding particle losses. An acceptable error for dipole differences between sectors is of the order of 10^{-4}. To achieve the nominal performance of the LHC accelerator, a maximum tune variation of ±0.003 tune units can be tolerated. For the commissioning with low intensity beams, acceptable bounds are up to 30 times higher [1] namely ±0.09 tune units. For the quadrupole-dipole integrated field ratio, the above requirements can be translated in the very tight windows of 6 ppm and 180 ppm, for nominal and commissioning performance respectively [2].

It is also necessary to forecast and correct the sextupole and decapole multipoles in the LHC main dipole magnets. The tolerances of the sextupole and decapole correction are calculated from the beam requirements [3] and these hence provide a specification for the forecasting mechanism. These calculations [4] yield the tolerances shown in Table 1.

To achieve these tolerances, the LHC is equipped with a hybrid control system consisting of beam based feed back and feed forward control. The feed forward control system is known as the Field Description for the LHC (FiDeL) which forecasts the main field and harmonics of the magnetic elements. This prediction is based on a model the parameters of which are determined with magnetic measurements at warm and at cold.

Table 1: The particle injection harmonic tolerance for commissioning and for nominal operation calculated from the beam requirements (values are shown in units).

	commissioning	**nominal operation**
b_3	0.35	0.02
b_5	-	0.1

FiDeL requires testing before LHC runs. To this end, CERN launched a dedicated measurement campaign, carried out in October and November 2007 in the SM-18 test station. The main aim of these tests was to verify whether FiDeL can:

1) accurately generate the current ramps of the main superconducting magnets which would produce the expected magnetic fields and therefore keep the B_2/B_1 and B_1/B_1 ratios well within the limits for the machine operation.

2) accurately generate the corrector current ramps to compensate the sextupole and decapole field errors in the main dipoles.

FiDeL is composed of static and dynamic field models that are based on the wealth of series magnetic measurements performed during magnet production [5, 6]. In practice, the model is formed by a set of equations and a table of parameters which are programmed within the LHC Software Architecture (LSA) [7].

This report presents the test campaign performed to track the main field and the multipoles of the selected LHC dipole and quadrupole magnets. We report the techniques developed to power the magnets, the instrumentation and data acquisition setup, the calibration procedure and data reduction employed as well as the results obtained. So as to test the system integrity, the whole chain of systems is controlled by LSA as will be done during standard operation in the CERN Control Centre (CCC).

2. MEASUREMENT SETUP AND CHARACTERISATION

2.1 - Magnet Characterisation

For this measurement campaign, two dipoles (MB2624 and MB2598) and a quadrupole (SSS064) were respectively installed on the test benches F2, A2 and B2 in SM-18. Each magnet was equipped with a rotating coil measurement system [8].

In the FiDeL static domain, MB2624, MB2598 and SSS064 were first characterized by measuring them during a stepped cycle (loadline cycle) of 10A increments up to 3000A and steps of 200A thereafter with the coils in rotating mode in the standard compensating mode. A typical loadline cycle is shown in Figure 1. These characterisation cycles were preceded by a pre-cycle with a ramp-up of 10A/s to nominal current (11850A), a waiting time of 1000s at this current and a subsequent ramp down of 10A/s. The pre-cycle was used to put the magnets in a known magnetic state. This characterisation cycle provided a much more detailed data set of the multipole variation along the powering cycle compared to that obtained during series magnetic measurements that were performed between 2002 and 2007.

In the FiDeL dynamic domain, the magnets were characterised with an LHC cycle (Figure 2) which in fact is a simulation of the real cycle of the machine. The LHC cycle has a ramp-up of 10A/s to injection current of 760A with a duration of 1000s on the injection plateau. This is followed by a standard LHC PELP (Parabolic Exponential Linear Parabolic) ramp, a 1000s flat-top plateau at the nominal current of 11850A, and a ramp-down to minimum current (350A) at 10A/s. The LHC cycle was preceded by a pre-cycle as described above.

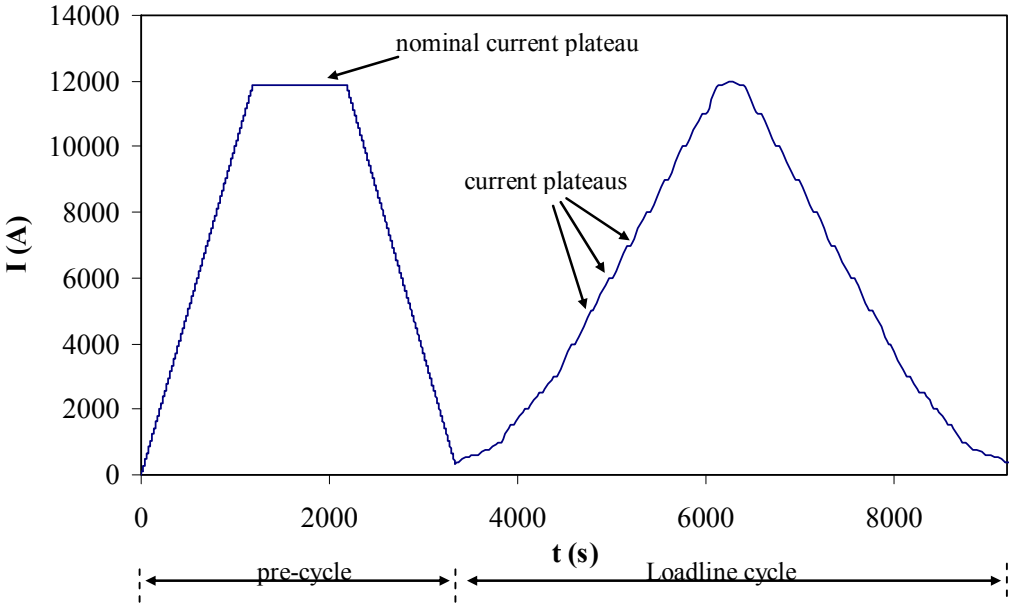

Figure 1: The loadline cycle

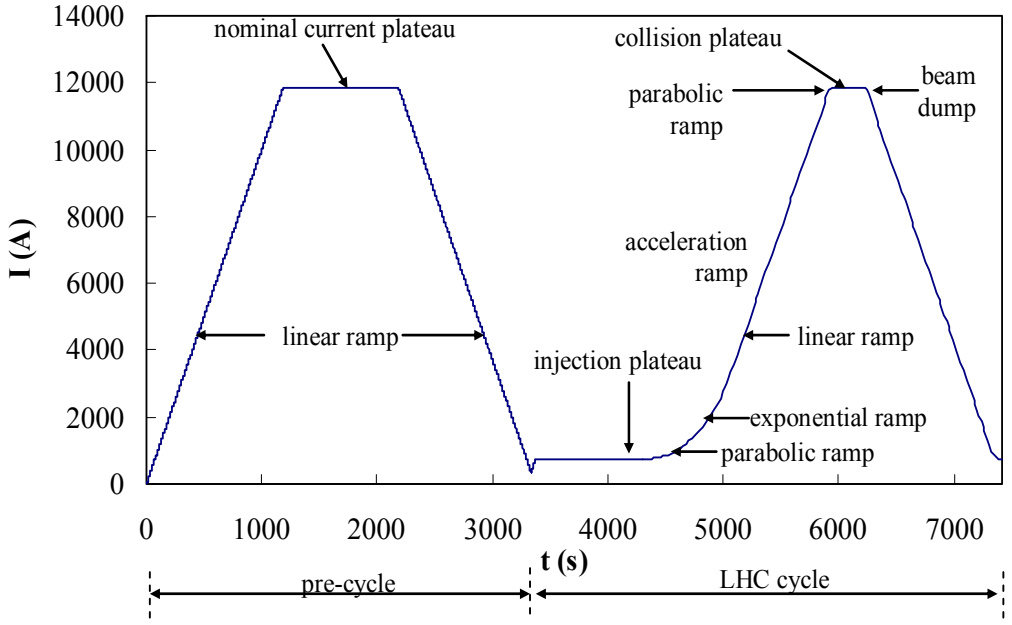

Figure 2: The standard LHC cycle

The coils were set at the standard magnetic measurement position which covered the magnetic lengths of the dipole magnet and that of the correctors. So as to eliminate errors due to sensitivity variation along the sector covering the correctors, the latter were characterised with a loadline cycle at the standard magnetic measurement position. The variation of the corrector strength as a function of the coil longitudinal position can be found in Appendix D.

The data set obtained from the characterisation measurement was treated in order to compensate the latency of the rotating coil measurements during the multipole decay on the current steps of the loadline [9]. The extraction of the static FiDeL parameters [5] was based only on the ramp-up data. In summary, care was taken that the measurement conditions and the magnet characterisation were as favourable as possible to exclude most systematic errors from the chain.

2.2 - Instrumentation

Pick-up coils were used in static mode for the B_2/B_1 and B_1/B_1 tracking and in rotating coil mode for the sextupole and decapole compensation. The same electronic systems were used for both configurations.

2.2.1 - Measurement Coils

Shafts co-h027, co-h028 and co-h30, co-h29 were installed in the apertures of the dipole magnets MB2624 and MB2598, respectively. They are made up of 13 ceramic segments (sectors) which provide the necessary rigidity for mounting two tangential, A and E, and one central, C, pick-up coils of 36 turns each. A simple schematic of the shafts is given in appendix B. The absolute signal is usually obtained from the reading of a signal of a single coil and is used for the determination of the main field component whilst the compensated signal is obtained as a combination of the signals of different coils, and is used for the determination of the field errors. The magnetic area of each of the coils is approximately 0.352 m^2/coil, their length 1.15 m/coil and between them there is a 110 mm gap which houses the rotating bearings and the cable inter-connects.

To measure the quadrupole field, shafts co-h35 and co-h36 were installed in apertures 1 and 2, respectively, of SSS064. These shafts are made up of 6 sectors each carrying 5 coils, namely A, B, C, D and E, of 64 turns each. The magnetic surface of each of the coils is approximately 0.381 m^2/coil, their length 0.7 m/coil and the gap between them is 110 mm. The surface vector of both dipole and quadrupole coils was set parallel to the direction of the main field by placing the coils at 0° for the dipoles and rotating the shafts by 45° with respect to the vertical plane of the magnet in the case of the quadrupoles.

2.2.2 - Data Acquisition System

The core of the acquisition system is a series of VME-PDI's (Precision Digital Integrators). In stationary mode, the integrators measure the flux change linked with the coils during magnet ramps. They are triggered at 1Hz by an external, frequency controlled function generator used to eliminate the difference between the integration time and the current given by the power supply. The PDI's are set with a fixed gain and are configured and read-out by a Sun Ultra workstation through a MXI interface to a VME-processor card in the VME crate. The system can be seen as a generic voltage acquisition system that delivers digitized values of the input voltage channels averaged over the integration time as defined by the external trigger. The trigger is sent in series from the first integrator to the last integrator with a very small delay. From the last integrator the trigger is inverted and transformed into a rectangular signal by the power supply trigger box and then sent to the power supply to read the current. The measurement is performed at the same time

for both apertures.

The same electronic VME-PDI system is also used in rotating mode except that the triggering is made by an angular encoder, the shafts are rotated at about 1Hz by a Twin Rotating Unit (TRU) and variable gains are used in the PDIs [8]. Each of the TRUs consists of a stepping motor with a 7:1 reduction gearbox and is remotely controlled by a data acquisition software system. The angular encoder has 4096 counts per revolution (of which 256 are used for the Fourier Transform) and its housing is rigidly connected to an electronic inclinometer giving an absolute reference for the 'zero' orientation of the encoder.

2.3 - Magnet Control Using LSA

LSA is the high level LHC controls software [7] that implements FiDeL in the LHC control system to convert the normalized magnet excitations into power supply currents, predict the field harmonics in the main magnets and distribute the appropriate corrections.

LSA is a common framework for development of high level control applications. It consists of a set of interdependent modules, providing a coherent set of functionalities, from the lowest level services up to the client applications. The LSA software stack is organized in 3 logical tiers: the resource tier consists of the database and the accelerator physical devices; the middle-tier is made up of the logic of the system; and the client tier represents the graphical user interface.

Several applications based on LSA core have been used to drive the tests. The most important one is 'Generation', which allows preparing current settings for the magnets, for a given supercycle. The generation module uses magnet curves I(B), and harmonic curves $b_n(I)$ which include the static FiDeL model effects. The dynamic model is implemented separately to predict the decay and snapback.

The application 'Calibration Curves Generator' uses the FiDeL model to generate the magnet curves. 'Equip State' and 'Equip Monitor' are used to interact with power converters (switch on/off, load settings, start, etc.) and monitor process variables (i.e. power converter currents) during the experiments. The system is designed to allow the running of several power converters at the same time with a very good accuracy. In this case, this is applied to the main bend and the corrector circuit. In addition, the standard sequence of commands is performed using the LHC sequencer.

3. MAIN FIELD TRACKING

3.1 - Measurement Cycles

The main field tracking accuracy was measured in several test runs. For the measurement of the field strength, the coils were kept stationary and were used in a flux meter configuration to measure the magnetic field variation through the voltage induced by the change in linked flux. In this measurement mode the coils do not provide an absolute field value, but only the field changes with respect to the initial value of the magnetic field.

Each run consisted of the respective current cycles simultaneously performed on the dipoles (MB2624 and MB2598) and on the quadrupole (SSS064). A typical current run consisted of a pre-cycle and several (ranging from one to three) standard LHC cycles chained all in supercycles, with no interruption. The effect of different pre-cycle flat top current was also tested during these series tests. An example of a supercycle used to power magnets MB2624, MB2598 and SSS064 is plotted in Figure 3.

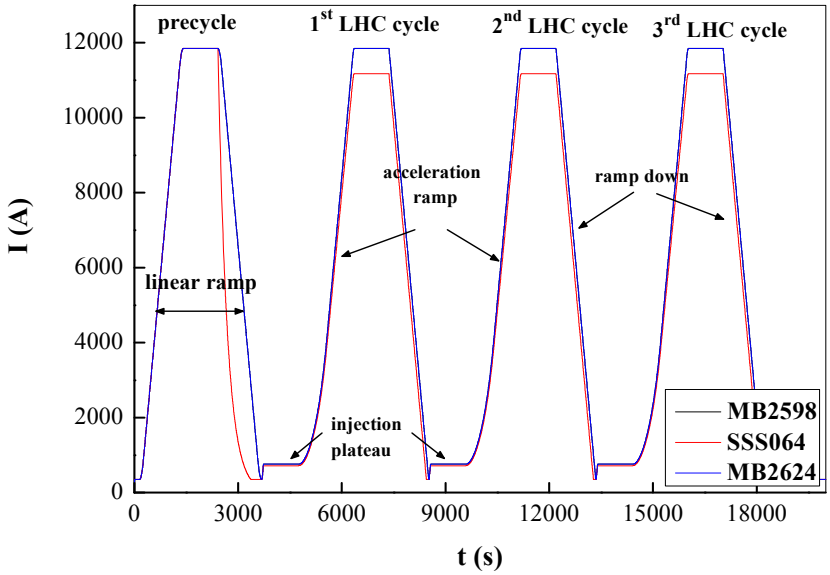

Figure 3: An example of current cycle (supercycle) loaded to dipoles MB2624 and MB2598 and to quadrupole SSS064 during October 2007 Tracking Campaign. The current supercycle consists of a pre-cycle at 12 kA and 3 successive standard LHC cycles.

During the October 2007 tracking campaign 10 supercycles (tracking test runs) were performed. These runs were preceded by a total of 9 pre-cycles (with current plateaus at 12 kA or 5 kA), while a total of 22 LHC cycles were performed. The tracking of the field strength between all three magnets was tested in 3 of these runs, whilst for the remaining 7 runs only one dipole and the quadrupole were powered up. The full list of tracking runs performed is shown in Table 2.

Table 2: List of tracking tests and magnets tested during October-November 2007 Tracking Campaign.

Date of measurement	Local time	Magnets tested	Number of precycles (and current plateau)	Number of LHC cycles
Wed 17/10/2007	14:28	MB2624 - SSS064	1 (12kA)	1
Thu 18/10/2007	13:09	MB2624 - SSS064	1 (12kA)	1
Thu 18/10/2007	15:32	MB2624 - SSS064	1 (12kA)	1
Fri 19/10/2007	10:40	MB2624 - SSS064	1 (12 kA)	3
Wed 24/10/2007	10:30	MB2624 - MB2598 - SSS064	1 (12 kA)	3
Thu 25/10/2007	09:20	MB2598 - SSS064	1 (12 kA)	1
Mon 12/11/2007	10:34	MB2624 - MB2598 - SSS064	1 (12kA)	3
Mon 12/11/2007	18:41	MB2624 - MB2598 - SSS064	1 (12kA)	3
Tue 13/11/2007	09:50	MB2624 - MB2598 - SSS064	1 (5kA)	3
Tue 13/11/2007	14:34	MB2624 - MB2598 - SSS064	no pre-cycle	3

3.2 - Full Description and Results of a Typical Run

In this section, we quote the measurements taken during the cycles performed on Friday 19/10/2007 and we describe the results of the analysis. During this run, the main field tracking was tested between dipole MB2624 and quadrupole SSS064. The magnets were excited with a pre-cycle at 12kA followed by three standard LHC cycles as shown in Figure 4.

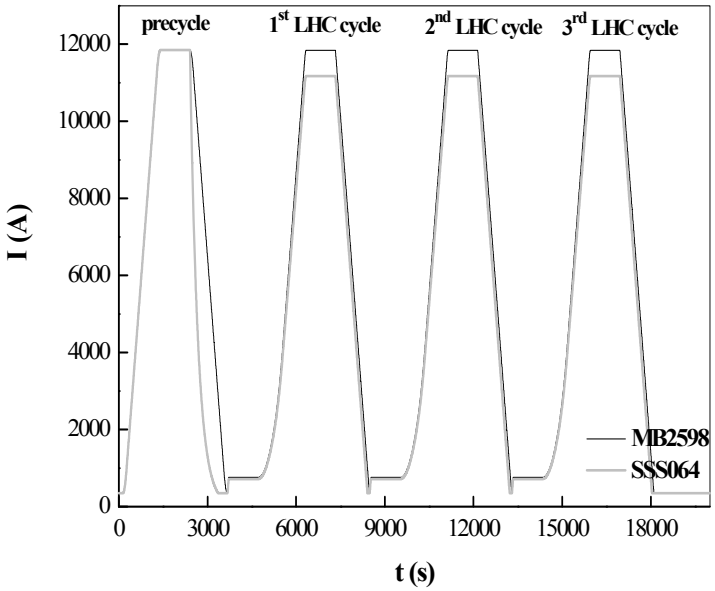

Figure 4: Graph of the supercycle loaded to dipole MB2624 and to quadrupole SSS064 for the tracking test performed on Friday 19/10/2007. The current cycle consisted of a pre-cycle at 12 kA and 3 successive standard LHC cycles.

Below we will present the results of analysis only for the first of the three LHC cycles performed. The measured data were analyzed following the steps described in Appendix A. The calculation of B_2/B_1 ratio was confined to the ramp-up part of the LHC cycles, i.e. we didn't analyze the pre-cycles or the ramp-down. Figure 5a shows the plateaus and ramp-up of the first current cycle for the dipole and quadrupole. We plot also the ratio of quadrupole to dipole current as a function of time.

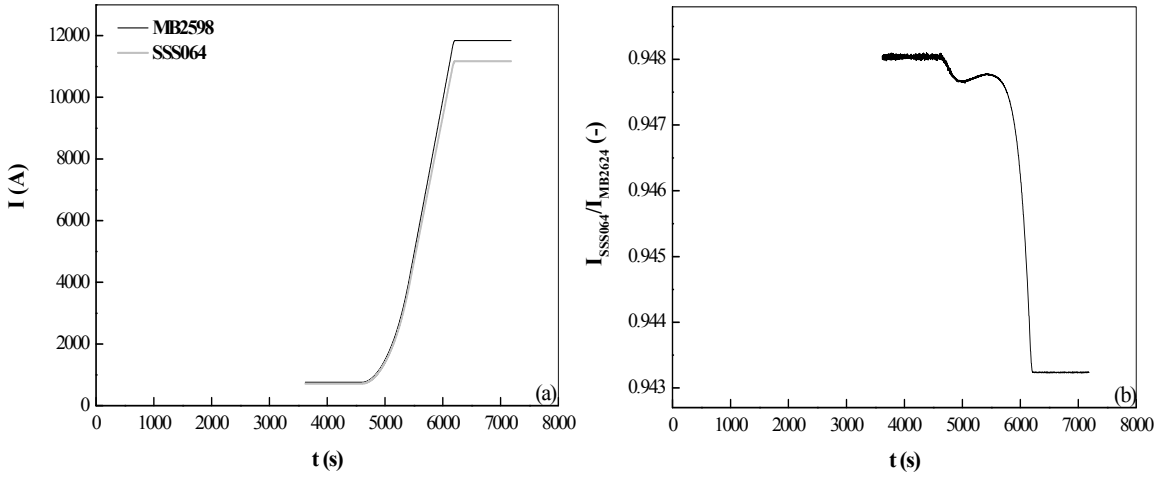

Figure 5: (a) First LHC current cycle and **(b)** ratio of quadrupole to dipole current driving MB2624 and SSS064 during tracking test performed on Friday 19/10/2007.

In Figure 6 we plot the voltage signals picked-up from shafts co-h27 and co-h35, installed in apertures 1 of MB2624 and SSS064 respectively, during the ramp-up phase. We individually plot the signals measured on each sector connected to the acquisition system. In the case of the main dipole field the signal comes from the top coil (A) for each of the sectors s0001 through sector s2223. For the main quadrupole field the absolute signal is obtained as the sum of signals coming from the two outermost coils, namely coils A and E, for each of the sectors s0203 through s1011. This is done so that the coil is only sensitive to the quadrupole field and the results are not influenced by the transverse position. The maximum values of the measured voltages were found to be approximately equal to 0.25 V and 0.45 V (in absolute values) for the dipole and the quadrupole, respectively. These maximum voltage values were measured on the central coils.

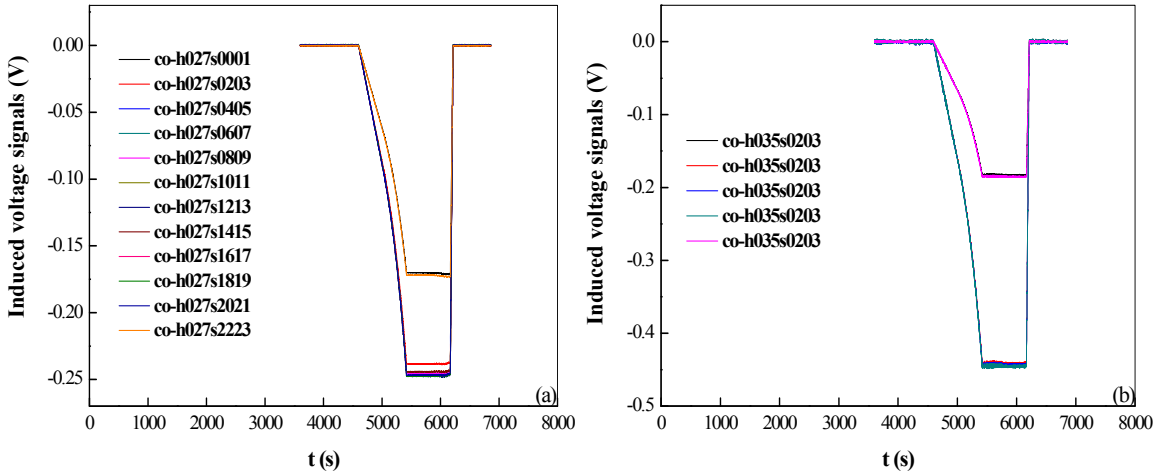

Figure 6: Induced voltage signals during the LHC cycle ramp-up as measured **(a)** on sectors s0001 through sector s2223 of shaft co-h027 installed in aperture 1 of dipole magnet MB2624 and **(b)** on sectors s0203 through sectors s1011 of shaft co-h35 installed in aperture 1 of quadrupole magnet SSS064.

The typical noise levels of the induced voltages on the sectors of dipole MB2624 and of quadrupole SSS064 are shown in Figure 7. We plot the measured voltages during the periods of constant current, i.e. at flat-bottom and at flat-top. During these phases of the cycle the voltage should be zero, and any deviation is due to voltage offsets and electronic or electromagnetic noise.

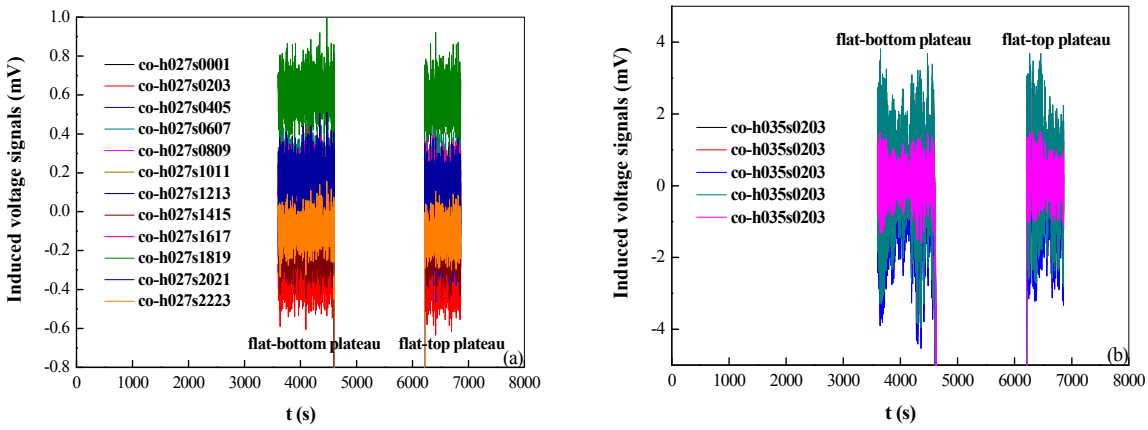

Figure 7: Coil signals during flat-bottom and flat-top (zero ramp-rate) measured on **(a)** sectors s0001 through sector s2223 of co-h27 installed in aperture 1 of MB2624 and **(b)** sectors s0203 through sector s1011 of co-h35 installed in aperture 1 of SSS064.

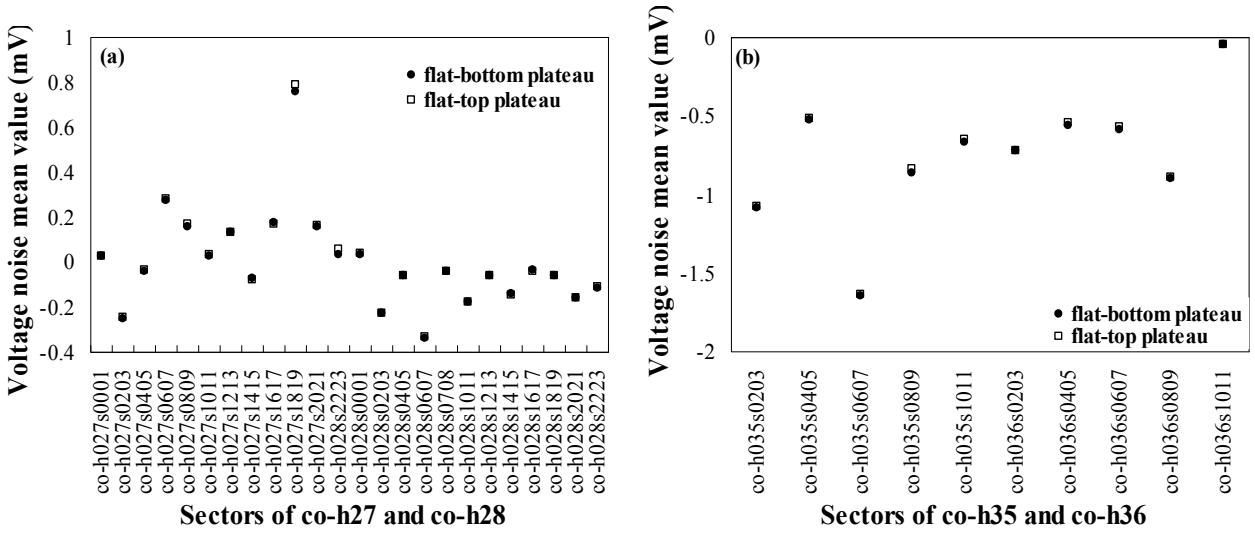

Figure 8: Calculated mean values of the voltage noise during flat-bottom and flat-top for all signals measured on **(a)** sectors s0001 through s2223 of shafts co-h027 and co-h28 installed in apertures 1 and 2 of dipole magnet MB2624 and **(b)** sectors s0203 through s1011 of shafts co-h035 and co-h36 installed in apertures 1 and 2 of quadrupole magnet SSS064.

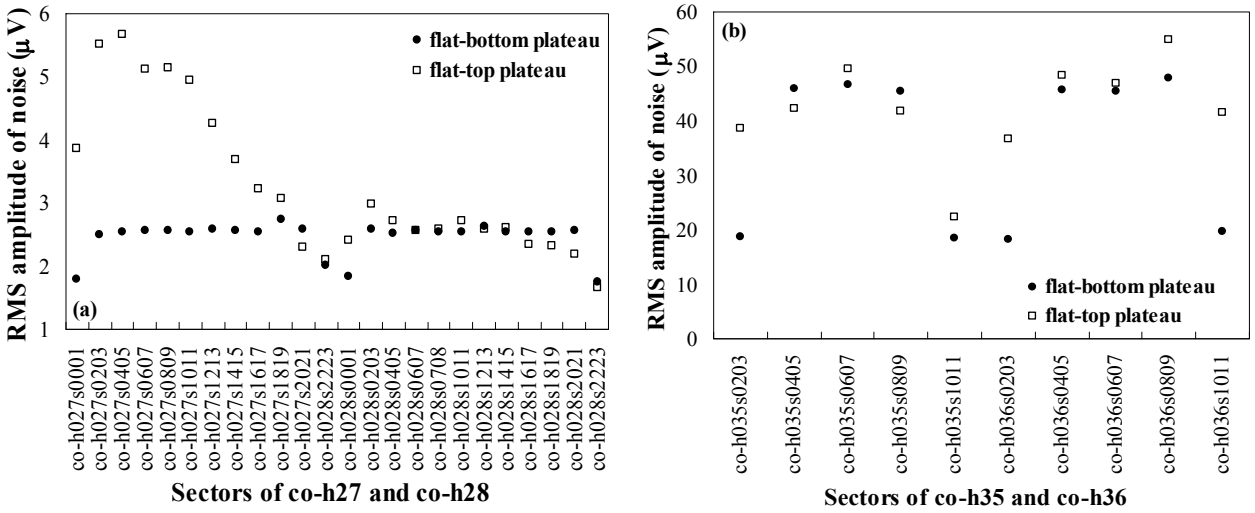

Figure 9: Calculated rms amplitude of the voltage noise during flat-bottom and flat-top for the signals measured on **(a)** sectors s0001 through s2223 of shafts co-h027 and co-h28 installed in apertures 1 and 2 of dipole magnet MB2624 and **(b)** sectors s0203 through s1011 of shafts co-h035 and co-h36 installed in apertures 1 and 2 of quadrupole magnet SSS064.

We observe that the mean value and the rms amplitude of the noise differ from coil to coil for both the dipole and the quadrupole. In Figures 8 and 9 we give the mean values and the rms amplitudes of the voltage noises for all coil signals. These values were measured during the flat-bottom and flat-top plateaus, where the current is constant and the voltage signal should ideally be zero[ℜ].

For the main dipole the mean values of the noise remain constant during the whole

[ℜ] Any correlation of the noise to the power converters was checked and assumed as insignificant. The noise in our case is that of electronic or electromagnetic nature.

measurement, ranging from some μV to 0.3 mV. Only the voltage signal measured on sector s1819 of co-h027 exhibits a mean noise value of approximately 0.8 mV. On the other hand, the rms amplitude of the noise exhibits a current dependence with its larger values appearing for the higher currents. The rms values of the noise for all sectors of shafts co-h27 and co-h28 are of the order of 1-6 μV. For the quadrupole the noise mean values of the voltage signals are current independent as well, unlike earlier observations [10], and range from some μV to 0.2 mV. The corresponding rms values are larger than the rms values of the dipole's voltage noises and are of the order of 20 – 60 μV.

For the calculation of the dipole and quadrupole field strengths the elimination of the noise from the measured voltage signals was necessary. Thus, the noise mean values were removed from each coil signal by means of a linear interpolation with the current, following [10]. The steps of the noise removal are quoted explicitly in Appendix A. However, the method of eliminating the voltage noise from the measured voltage signals, although effective was not completely successful. A dedicated error study, quoted in Appendix C, showed that the residual voltage noise, when integrated, leaded to a statistical uncertainty of $1.6 \cdot 10^{-3}$ T·m for the main dipole field and to an uncertainly of $1.2 \cdot 10^{-3}$ T·m for the main quadrupole field. Both statistical uncertainties are given at nominal current.

Finally, in Figure 10 we give the instantaneous values of the ratio B_2/B_1 calculated from the measured data. We plot, also, at indicative points of the curves an estimate of the statistical uncertainty on the B_2/B_1 ratio, which we will call 'instrumentation error'. The estimation of the 'instrumentation error' is discussed in Appendix C and is due to residual voltage noise which could not be successfully removed from the measured voltages and was therefore integrated all along with the voltage signals. In Figure 10 the two innermost, solid lines define the maximum allowable variation of B_2/B_1 ratio for nominal operation which corresponds to a tune variation of ±0.003 tune units. The region between the two outermost solid lines defines the maximum allowable variation for commissioning operation, i.e. ±0.09 tune units.

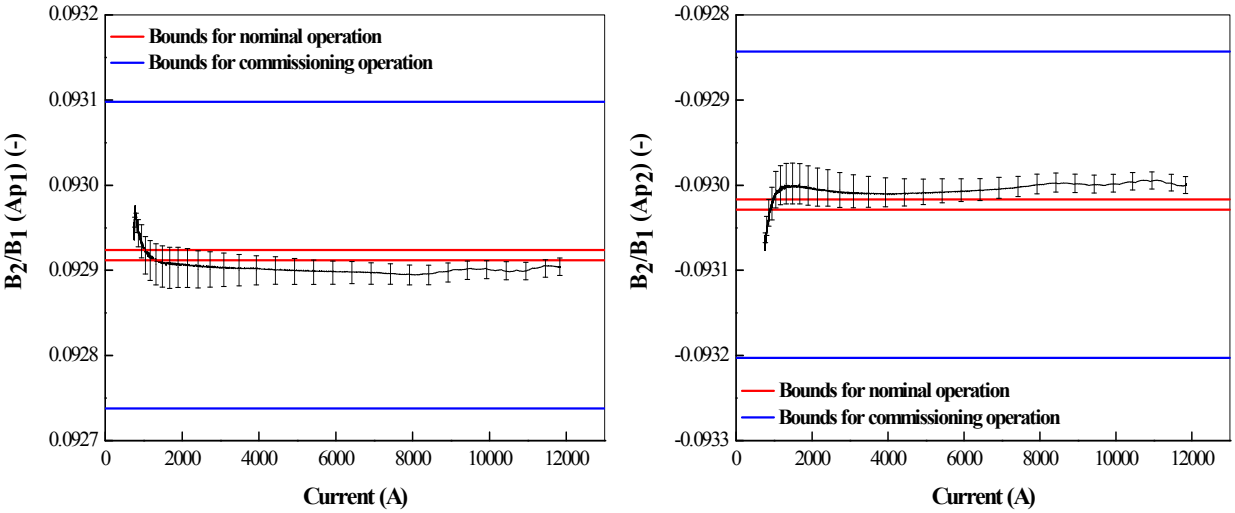

Figure 10: Ratio of quadrupole to dipole field strength for apertures 1 **(left)** and 2 **(right)** as a function of the dipole's current calculated from measurements during an LHC current ramp. The ideal ratio should be constant. The results obtained are compared to the specifications for nominal (innermost solid, red lines) and commissioning operation (outermost solid, blue lines). The 'instrumentation error' bars are also plotted at indicative points of the curves.

Results show that the B_2/B_1 ratio is definitely within the range to be achieved for commissioning operation and quite close to the range necessary to maintain the maximum

allowable tune variation to within $3 \cdot 10^{-3}$ as dictated for the nominal LHC performance. We observe that the 'instrumentation error' is not constant but exhibits a complex current dependence. Its values vary from $1 \cdot 10^{-6}$ to $2.5 \cdot 10^{-5}$ [ℜ] leading to an uncertainty of 0.01 to 0.25 units in our results which is comparable to the order of allowable variation of B_2/B_1 ratio for the machine's operation. The 'instrumentation error' reflects the limitations in the measurement accuracy that can be achieved as well in the compensation of the measurement uncertainties by the analysis method. 'Instrumentation error' values don't change from cycle to cycle since they depend only on the measurement configuration, and the values reported here apply to the whole campaign.

3.3. - Main Field Tracking Campaign Results

Figure 11 shows all the results of tracking measurement campaign. In these graphs we do not plot the 'instrumentation error' bars so as to limit the cluttering effect of having too many data in each graph. We plot the instantaneous values of ratios B_2/B_1 and B_1/B_1 calculated from measurements performed on apertures 1 of magnets MB2624, MB2598 and SSS064. In particular, we have included 21 curves for B_2/B_1 ratio coming from tracking of MB2624 with SSS064, 12 curves for B_2/B_1 ratio coming from tracking MB2598 with SSS064 and 13 curves for B_1/B_1 ratio coming from tracking MB2624 with MB2598.

Moreover, with the aim to verify the reproducibility of our results we calculated and plotted the cycle-to-cycle change of B_2/B_1 and B_1/B_1 ratios, indicated by $\Delta(B_2/B_1)$ and $\Delta(B_1/B_1)$. The cycle-to-cycle changes, $\Delta(B_2/B_1)$ and $\Delta(B_1/B_1)$, are calculated by subtracting the B_2/B_1 and B_1/B_1 ratios coming from each LHC cycle from the ratios coming from the last LHC current cycle performed during the Tracking Campaign (i.e. the 3rd LHC cycle of the test run performed on 11 November, 2007 at 14:34). Reproducibility can be verified in this way since current ramps were the same for all tests performed. For all cases the results are compared to the bounds for the maximum allowable variation of B_2/B_1 or B_1/B_1 ratio for nominal and commissioning operation.

In Table 3, we quote the average range of the calculated B_2/B_1 (or B_1/B_1) and $\Delta(B_2/B_1)$ (or $\Delta(B_1/B_1)$) ratios as they were extracted from the graphs of Figure 11. For the calculation of the average ranges we estimated the peak-to-peak amplitude of each curve and then we computed their average value. The ideal average ranges should be zero giving constant B_2/B_1 and B_1/B_1 ratios and zero variation of results from cycle to cycle.

Table 3: Average ranges of B_2/B_1 (or B_1/B_1) and $\Delta(B_2/B_1)$ (or $\Delta(B_1/B_1)$) ratios as extracted from graphs of Figure 11 (values are in units).

Magnets tested	**B_2/B_1 (or B_1/B_1) average range**	**$\Delta(B_2/B_1)$ (or $\Delta(B_1/B_1)$) average range (reproducibility from cycle-to-cycle)**
MB2624 – SSS064	0.358	0.11
MB2598 – SSS064	0.286	0.08
MB2598 – MB2624	1.238	0.53

[ℜ] The 'instrumentation error' is dimensionless since it represents the statistical uncertainly in B_2/B_1 ratio.

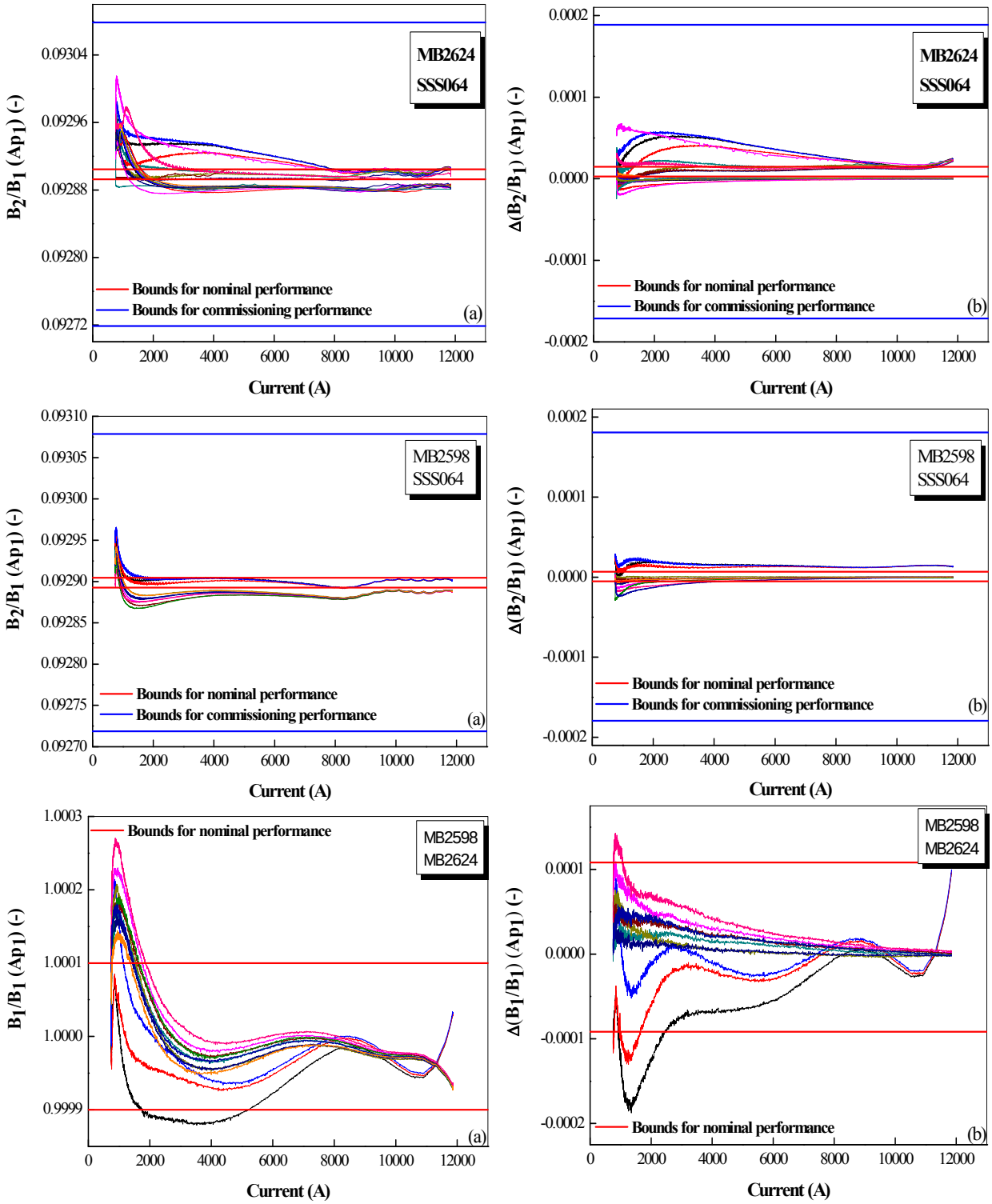

Figure 11: (Top) (a) Ratio of quadrupole to dipole integral field, B_2/B_1, and **(b)** cycle-to-cycle change of $B_2/B1$ for aperture 1 of MB2624 and SSS064, **(middle) (a)** ratio of quadrupole to dipole integral field, B_2/B_1, and **(b)** cycle-to-cycle change of $B_2/B1$ for aperture 1 of MB2598 and SSS064 and **(bottom) (a)** ratio of dipole to dipole integral field, B_1/B_1, and **(b)** cycle-to-cycle change of B_1/B_1 for aperture 1 of MB2598 and MB2624. All results have been calculated from measurements during LHC current ramps performed in October 2007 Tracking Campaign. The bounds for nominal (innermost solid, red lines) and commissioning operation (outermost solid, blue lines) are plotted too.

From the data of Table 3 we see that the range of variation of the quadrupole-dipole ratio is constant to approximately ± 0.36 units when we track MB2624 with SSS064 and constant to ± 0.29 units when we track MB2598 with SSS064. We recall that the commissioning tolerances for the tune are $9 \cdot 10^{-2}$, i.e. 1.8 units for the ratio of integral quadrupole to dipole field and hence our results are well within the target band. For nominal performance the ratio of quadrupole to dipole field has to be constant to 0.06 units to achieve a constant tune of $3 \cdot 10^{-3}$; in which case our calculated values obtained span a larger range but with reproducibility from cycle to cycle very close to the very tight targets needed. Indeed it is not yet clear whether the initial behaviour observed (steep drop in B_2/B_1) is due to an artefact introduced to the measurement system or due to a less accurate FiDeL field prediction for the quadrupole.

Our calculations give the ratio of dipole-dipole field to be constant to approximately ±1.23 units while the target for the ratio of dipole-dipole integral field is ± 1 units. This means that the ratio of the dipoles field is mostly within the target band and most important, its reproducibility is well within ± 1 units

4. HARMONICS COMPENSATION

4.1 - Harmonic Correction using LSA

Harmonic correction in LSA is performed by using FiDeL to generate the harmonic curve that needs to be compensated (e.g. b_3 or b_5 of the dipole). The magnetic strength of the corrector is then obtained by using the harmonic curve and the ratio of the magnetic lengths between the dipole and the corrector. The corrector current is then obtained from the corrector magnetic strength by using the transfer function of the corrector as defined in FiDeL (known in LSA as the corrector calibration curve).

4.2 - The Test Setup

The compensation of the sextupole and decapole in the main magnets was performed by powering the sextupole (MCS) and decapole correctors separately in two dipole cold masses with the standard LHC cycle shown in Figure 2. The powering was performed using LSA as described above and was based on the FiDeL prediction as derived from detailed characterization measurements. The cycles performed for the compensation tests are shown in Table 4.

Table 4: The cycles performed for the sextupole and decapole compensation

Tracking Test	Magnets tested	Harmonic	Number of precycles (and current plateau)	Precycle ramp rate	Number of LHC cycles
October	MB2624 Ap1	b3	standard LHC cycle	10	5
October	MB2624 Ap1	b3	standard LHC cycle	50	1
October	MB2624 Ap2	b3	standard LHC cycle	10	3
October	MB2624 Ap2	b3	standard LHC cycle	50	1
October	MB2624 Ap1	b5	standard LHC cycle	10	3
October	MB2624 Ap1	b5	standard LHC cycle	10	1
October	MB2598 Ap1	b3	standard LHC cycle	10	5
October	MB2598 Ap1	b3	standard LHC cycle	50	1
October	MB2598 Ap2	b3	standard LHC cycle	10	3
October	MB2598 Ap2	b3	standard LHC cycle	50	1
October	MB2598 Ap1	b5	standard LHC cycle	10	3
October	MB2598 Ap1	b5	standard LHC cycle	10	1
December	MB2598 Ap1	b3	standard LHC cycle	10	4
December	MB2598 Ap2	b3	standard LHC cycle	10	2

4.3 - b3 Compensation

Figure 12 shows the dependence of the integral sextupole on current before and after correction. The red curves show the uncorrected harmonics whilst the blue curves show the harmonic component after compensation with the corrector. The latter are integral measurements of the harmonic over the full length including the dipole and the corrector. From the plot, it is evident that at this scale, the correction works to a high degree.

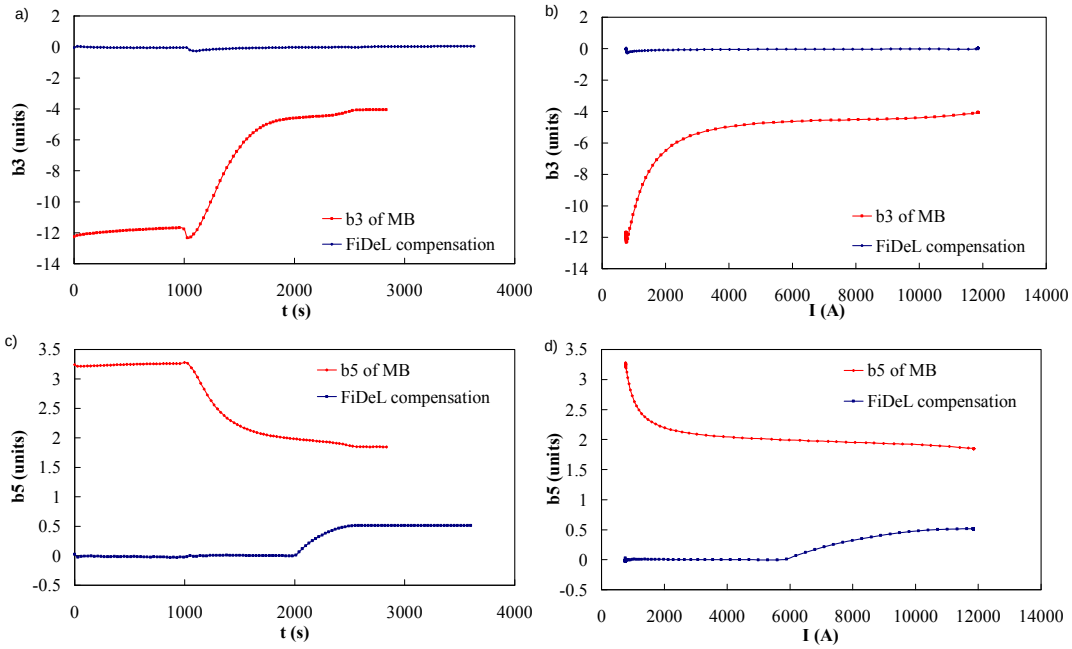

Figure 12: (**a, b**) Integral sextupole and (**c, d**) the integral decapole in aperture 1 of dipole MB2598 before correction (red) and after correction (blue) using the MCS and the MCD respectively in the cold mass.

Zooming in on the scale to examine the compensated sextupole further, some remnant features of the multipole variation can still be observed. Figures 13 and 14 show the measured integral sextupole in the two apertures of the two magnets in two subsequent cycles. The sextupole variation is of ± 0.25 units corresponding to a variation of about ± 10 units of chromaticity. What is most interesting, also in this case, is that the reproducibility is better than 0.1 units of sextupole corresponding to a chromaticity range of 5 units.

The origin of the features in the figures is as yet unclear. The range of variation of integral sextupole is small, not much larger than the measurement uncertainties, and systematic errors in the measurement of the sextupole in the dipole, or the gain of the MCS corrector, could explain some of the features observed. To verify this issue, we have tested the effect of a reduction of 2% of the parameter that sets the gain for the MCS corrector (see Figure 15). The hardware effect is to increase the field generated by the MCS. The integral sextupole, including compensation, is centred around zero, and has a much reduced range of ±0.15 units.

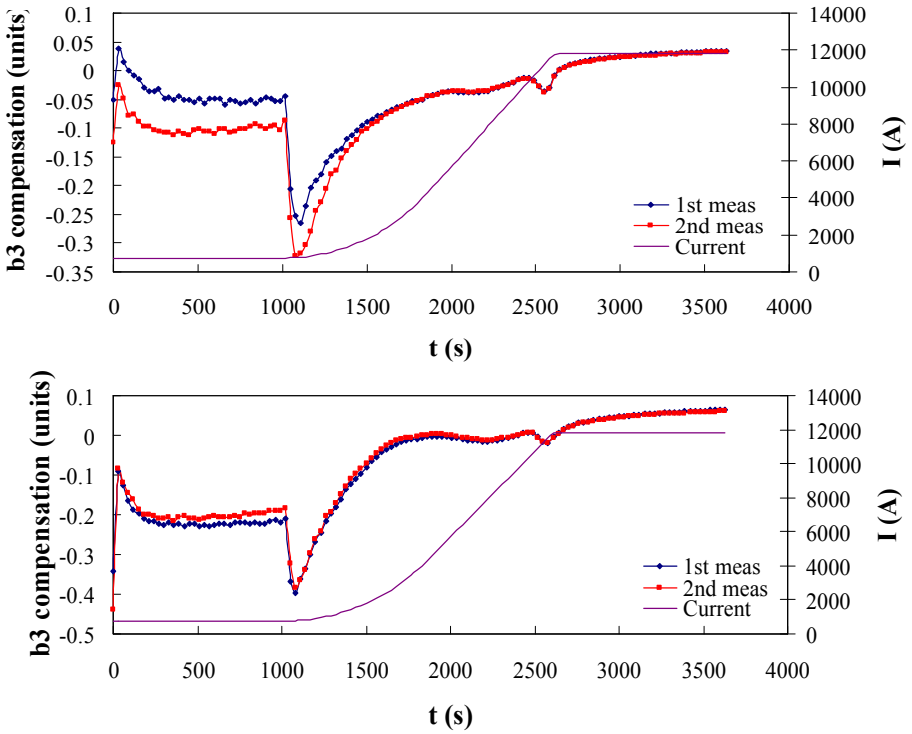

Figure 13: Remnant integrated sextupole in aperture 1 of MB2624 and MB2598 during two subsequent machine cycles

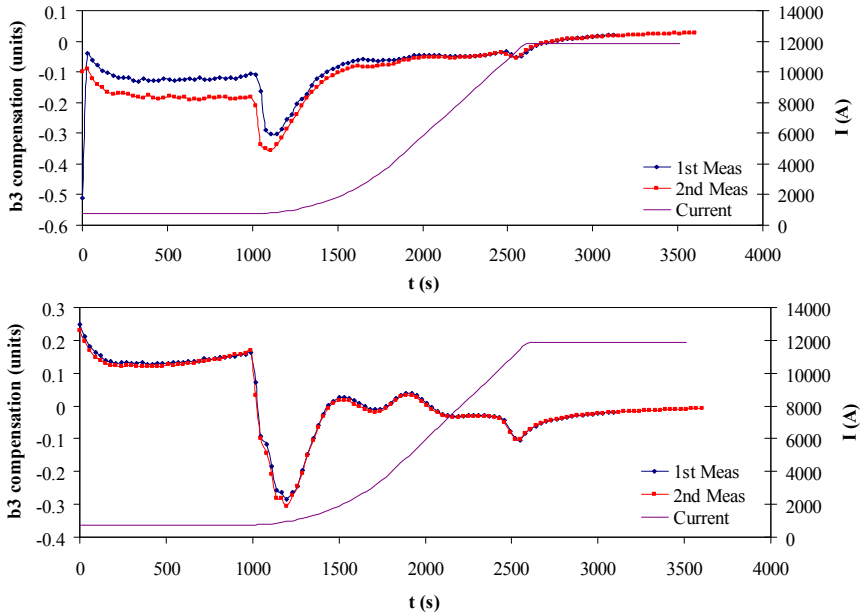

Figure 14: Remnant integrated sextupole in aperture 2 of MB2624 and MB2598 during two subsequent machine cycles

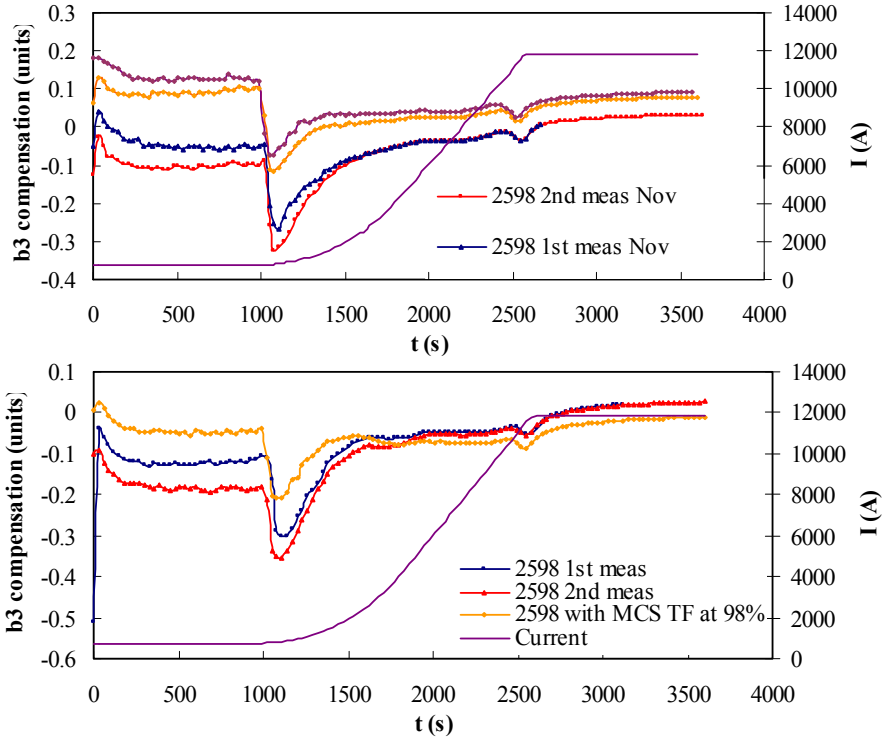

Figure 15: Integral sextupole in aperture 1 (above) and aperture 2 (below) of the dipole MB2598 during two machine simulation runs (red and blue curve) compared to the effect of changing arbitrarily the gain of the corrector magnet by 2% (green curve).

In the case of aperture 1, the corrector gain parameter was reduced further to 2.5%. The sextupole remnant variation in this case is very similar to what was obtained with a reduction of 2% in the gain parameter except that the average error shifts upwards by 0.05 units.

4.4 - b5 compensation

Zooming in on Figure 12 to examine the compensated decapole further, some remnant features of the multipole variation can still be observed. Figure 16 and 17 shows the measured integral decapole in the two apertures of the two magnets. The decapole variation is ±0.02 units with a reproducibility of 0.01 units. However, during the cycle, the maximum strength of the decapole magnets is reached and the harmonic is not corrected further. For magnet 2598 this occurs at 2000s for aperture 1 and does not occur in aperture 2. In the case of magnet 2624, this occurs at about 2500s for both apertures.

From series measurements performed at warm [11], it is known that the b5 component, for the whole dipole population, on average, is just at the specification limit. Therefore it is expected to have individual magnets reach their field strength. However, for b5 compensation over the whole machine, the corrector strength should be enough on average.

From beam dynamics, it is known that the b5 correction is only critical at injection. However, if correction of b5 would also be required at nominal operation a more complex control algorithm would be required to compensate for the variation of the average b5 in each sector.

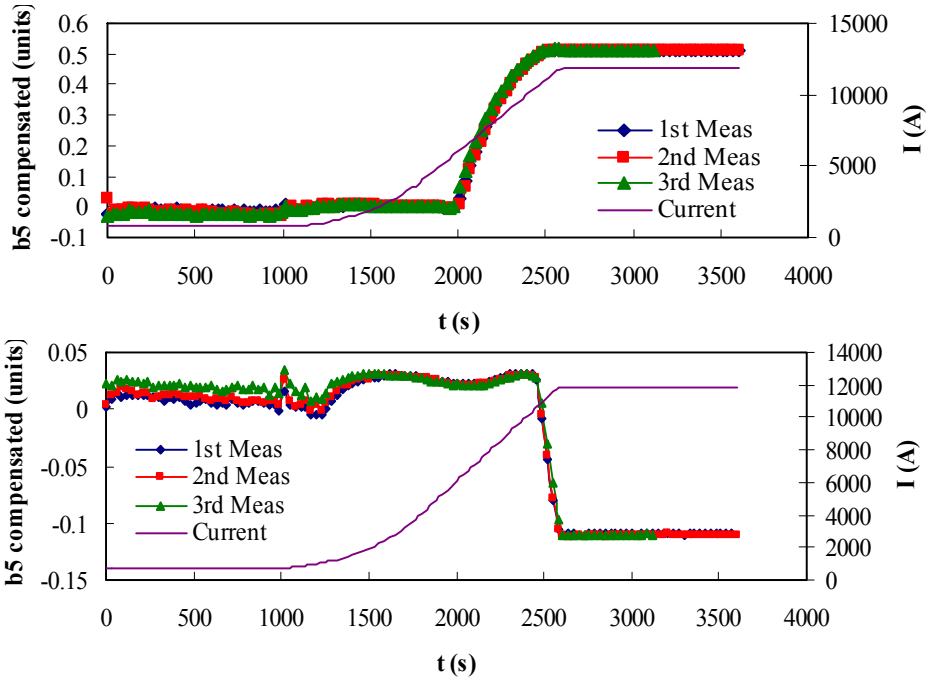

Figure 16: Remnant integrated decapole in aperture 1 of MB2624 and MB2598 during three subsequent machine cycles

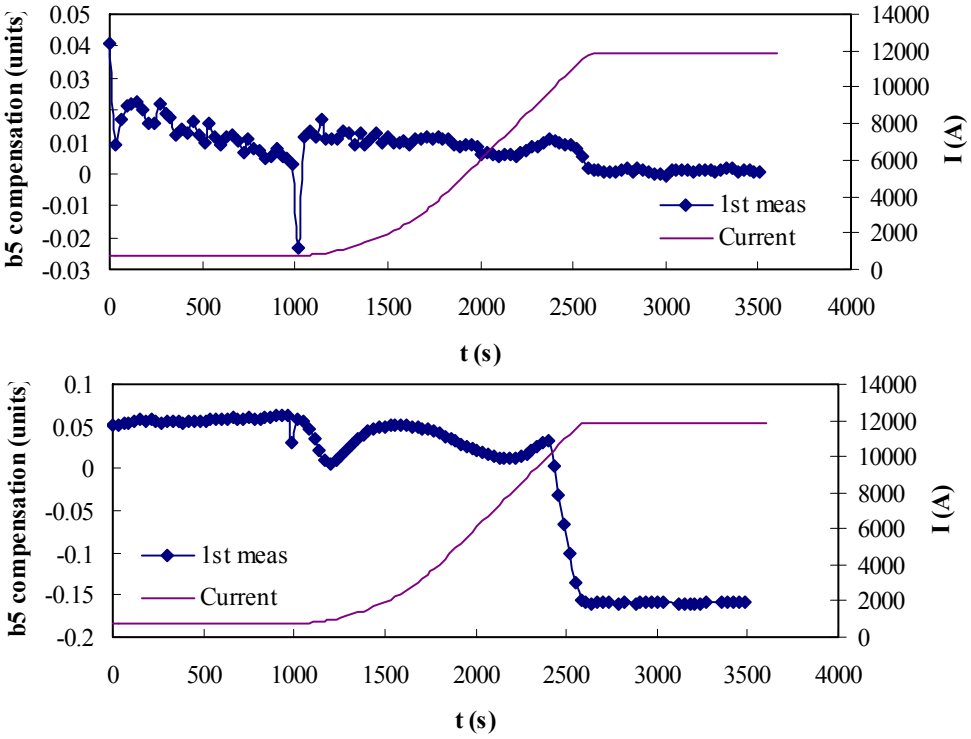

Figure 17: Remnant integrated decapole in aperture 1 of MB2624 and MB2598 during a machine cycle

5. CONCLUSIONS

The tracking experiments have demonstrated that the principle of FiDeL works well and that its implementation in LSA is working. Some effects are not yet understood but the indications are that these are within the tolerances.

The results for the main field tracking showed that dipole-dipole and dipole-quadrupole ratios can be kept constant within the range to be achieved for beam commissioning and quite close to the range necessary to maintain the maximum allowable tune variation for the nominal LHC performance. Moreover, we observed that the quality of our results improved considerably when we calibrated our results using rotating coil measurements. This technique is equivalent to correcting the calibration factors so as to eliminate errors introduced due to misaligned shafts with respect to the field axis and non-quantified effects of read-out electronics. Furthermore, the cycle-to-cycle reproducibility is very close to the tight targets needed.

We believe that the variation of the dipole-dipole and dipole-quadrupole ratios can be attributed to two factors: a) to a less accurate FiDeL description for the SSS064 quadrupole and b) to the 'instrumentation error' which reflects the limitations in the measurement accuracy that can be achieved as well in the compensation of the measurement uncertainties by the chosen analysis method. A dedicated error analysis study showed that instrumentation error is not constant but exhibits a complex current dependence. Its values vary from $1 \cdot 10^{-6}$ to $2.5 \cdot 10^{-5}$ leading to an uncertainty of 0.01 to 0.25 units in our results which is comparable to the order of allowable variation of B_2/B_1 ratio for the machine's operation. However, 'instrumentation error' values don't change from cycle to cycle since they depend only on the measurement configuration.

The sextupole and decapole compensation tests worked well with a maximum error swing of 0.3 units. The origin of remnant sextupole field after correction is still unknown. LSA timing issues were studied and solved so that each part of the model is suitably matched and launched precisely at the right time. The contribution of the corrector hysteresis was also calculated to be 0.05 units hence not being the cause of the remnant field.

One of the ideas is that the residual b_3 at the beginning of the ramp partly occurs because the snapback correlation varies slightly from magnet to magnet. However this does not explain why the 'ditch' takes 500s to recover.

Another cause of the remnant field could be due to the instrumentation. Whilst the magnet characterisation is performed with the rotating coil amplifier gains in variable mode, during compensation tests the amplifiers are place in fixed mode. The difference in the amplifier sensitivity of the two modes may contribute to the remnant field.

Another issue is that there seems to be a difference of about 0.2 units of b_3 between different loadlines performed at different times. The origin of this difference is unknown but the effect may be the source of the remnant sextupole field. A more detailed discussion about this issue can be found in Appendix E.

It should be noted that the tests to check out the powering history dependence of the decay were not completed due to technical problems. This dependence is planned to be tested in the next tracking test.

6. REFERENCES

[1] O. Brüning, "Accumulation and Ramping in the LHC", Proceedings of the Workshop on LEP-SPS Performance Chamonix X, 198-202, CERN-SL-2000-007-DI, 2000.

[2] V.Granata et al., "Magnetic Field Tracking Experiments for LHC", Proceedings to European Particle Accelerator Conference, Lucerne Switzerland July 2004.

[3] O. Brüning, "Accumulation and Ramping in the LHC", 10th Workshop on LEP SPS Performance, Chamonix X, pp. 198-202, Chamonix, France, January 2000.

[4] S. Fartoukh and O. Brüning, "Field Quality Specification for the LHC Main Dipole Magnets", LHC Project Report 501, CERN Geneva, Switzerland, October 2001.

[5] N. Sammut, L. Bottura, J. Micallef, "A Mathematical Formulation to Predict the Harmonics of the Superconducting LHC Magnets", Phys. Revs ST - Accel. Beams, Vol 9 No 1, 012402 January 2006.

[6] N. Sammut, L. Bottura, P. Bauer, T. Pieloni, J. Micallef, "Mathematical Formulation to Predict the Harmonics of the Superconducting Large Hadron Collider Magnets: Part II - Dynamic Field Changes and Scaling Laws", Phys. Revs ST - Accel. Beams - Vol. 10, No.8, 082802, August 2007.

[7] M. Lamont, L. Mestre, "LHC Era Core Control Application Software", Proceedings to the ICALEPCS'2005, Geneva, October 2005.

[8] J. Billan, L. Bottura, M. Buzio, G. D'Angelo, G. Deferene, O. Dunkel, P.Legrand, A. Rijllart, A. Siemko, P. Sievers, S. Schloss, L. Walckiers, "Twin Rotating Coils for Cold Magnetic Measurements of 15 m Long LHC Dipoles", IEEE Transactions on Applied Superconductivity, vol. 10, pp. 1422-1426, December 1999.

[9] N. Sammut, L. Bottura, W. Venturini Delsolaro, G. Deferne, "Dependence of the Static and Dynamic Field Quality of the LHC Superconducting Dipole Magnets on the Pre-cycle Ramp Rate", Proceedings to the European Particle Accelerator Conference, Genova, Italy, June 2008, in work.

[10] V.Granata et al., "Tracking and k-modulation measurements in String II", LHC Project Note 319, 2003.

[11] E. Todesco, B. Bellesia, L. Bottura, A. Devred, V. Remondino, S. Pauletta, S. Sanfilippo, W. Scandale, C. Völlinger, E. Wildner, "Steering Field Quality in the Main Dipole Magnets of the Large Hadron Collider", IEEE Transactions on Applied Superconductivity, vol. 14, pp. 177-180, June 2004.

APPENDIX A - DATA TREATMENT

Each measurement consists of reading an absolute and a compensated signal as delivered from each of the sectors of the shafts. The absolute signal is usually obtained from the reading of a signal of a single coil and is used for the determination of the main field component whilst the compensated signal is obtained as a combination of the signals of different coils, and is used for the determination of the field errors. For the main field tracking, only the absolute signals were considered. In the case of the main dipole field the signal came from the top coil (A) for each of the sectors s0001 through sector s2223. For the main quadrupole field the absolute signal was obtained as the sum of signals coming from the two outermost coils, namely coils A and E, for each of the sectors s0203 through s1011. In the latter's case, the symmetry in the position of coils A and E was exploited for improving the measurement accuracy and minimizing the effects of a displacement of the shaft with respect to the magnetic centre of the magnet.

The absolute signals $\Delta V_{i,s,a}$ constitute the voltage increments between two successive triggers spaced by a time interval Δt_i. i is the time-stamp at the which measurements were taken, s indicates the numbering of the sectors of the shafts connected to the acquisition system (12 for the main dipoles and 5 for the main quadrupole) whilst a indicates the magnet's aperture. All fixed coil measurements were first normalized with the gains of the amplifier chains. The absolute values of the voltage increments then were:

$$\Delta V_{i,s,a} = \frac{\Delta V_{\text{PDI Output}_{i,s,a}}}{G_{PDI}} \tag{A1}$$

where G_{PDI} is the gain of the instrumentation amplifier. The PGA's were set at a fixed gain of 100 for the main dipole signals and at a gain of 200 for the quadrupole coil signals.

An important step in the data reduction is the removal of any voltage noise from the voltage signals. The integrator reading of the coils' voltage can be affected by a voltage offset caused by the cable interconnections and the amplifier stages. In our analysis the voltage noise was measured during periods of constant current during the LHC cycles, i.e. at flat-bottom and at flat-top plateaus, where the voltage signals read from the coils should ideally be zero. The mean noise values were calculated as:

$$\Delta V_{off,s,a} = \frac{\sum_{i=1}^{N} \Delta V_{i,s,a}}{N} \tag{A2}$$

where i indicates the N measurements taken during a flat-bottom or flat-top plateau. For each LHC cycle performed, for each magnet aperture and for each sector we calculated two mean noise values, $\Delta V_{off,s,a_{FB}}$ and $\Delta V_{off,s,a_{FT}}$, coming respectively from the flat-bottom and flat-top plateaus. For obtaining the corrected voltage signals per sector and aperture, $\Delta V_{corr\,i,s,a}$, the calculated mean values were removed from the measured voltage signals $\Delta V_{i,s,a}$ by using a linear interpolation with the current [10], namely:

$$\Delta V_{\text{corr}_{i,s,a}} = \Delta V_{i,s,a} - \left[(1-\xi) \cdot \Delta V_{\text{off},s,a_{FB}} + \xi \cdot \Delta V_{\text{off},s,a_{FT}} \right] \tag{A3}$$

where ξ is a function of current given by:

$$\xi = \frac{I - I_{FB}}{I_{FT} - I_{FB}} \tag{A4}$$

ξ varies linearly from 1, when $I=I_{FT}$, to 0, when $I=I_{FB}$. I_{FB} and I_{FT} stand for the current at flat-bottom and flat-top plateaus respectively.

The flux increments $\Delta\varphi_{i,s,a}$, i.e. the flux changes with respect to the initial flux value picked-up by each of the sectors at each time interval Δt_i were then calculated as the time integral of the corrected induced voltage values, numerically implemented as:

$$\Delta\varphi_{i,s,a} = -(\Delta\varphi_{i-1,s,a} + \Delta V corr_{i,s,a} \cdot \Delta t_i) \tag{A5}$$

The method of eliminating the voltage noise from the measured voltage signals, although effective was not completely successful. For this reason, the voltage increments in time had to be carefully integrated. We confined our integration only to the ramp-up phase so as to avoid integrating the residual noise in the plateau regions. The integration started in the beginning of the ramp-up phase of the LHC cycle at which we set the initial value of the flux equal to zero, namely $\Delta\varphi_{o,s,a}=0$.

The increments in the local field strength, $\Delta B^1_{i,s,a}$ and $\Delta B^2_{i,s,a}$, for each magnet aperture and each sector were obtained using the calculated local flux change and the coil calibration coefficient (sensitivity factor) to the desired harmonic K_n:

$$\Delta B^n_{i,s,a} = \frac{\Delta\varphi_{i,s,a}}{K_n}, \quad n = 1, 2 \tag{A6}$$

The sensitivity factor K_n of a single coil for the harmonic of order n, with filamentary windings, located at positions z_1 and z_2 in the complex plane, at any instant is:

$$K_n = \left(\frac{NLR_{ref}}{n}\right)\left\{\left(\frac{z_2}{R_{ref}}\right)^n - \left(\frac{z_1}{R_{ref}}\right)^n\right\} \tag{A7}$$

where N is the number of turns, L the length of the coil along the magnet axis and R_{ref} is the reference radius taken to be 17 mm for the LHC. For a perfect tangential coil the sensitivity factor reduces to the purely imaginary number:

$$K_n^{tang} = -i\frac{2NLR_{ref}}{n}\left(\frac{R_c}{R_{ref}}\right)^n \sin\left(\frac{n\Delta}{2}\right) \tag{A8}$$

where R_c is the radius of centre of gravity of the winding and Δ is the coil opening angle. In case of a dipole field (n=1) and for a coil perpendicular to the field, the above expression resulted in the coil surface. For the main quadrupole (n=2) where the absolute voltage signals came from a series connection of two coils the total sensitivity was computed as the algebraic sum of all coils sensitivities. The $\Delta B^2_{i,s,a}$ values calculated from the combination of equations (A6) and (A8) refer to the R_{ref} radius. In Tables B1 – B6 of Appendix B we summarize the length, the position in the shaft and the coil sensitivities for all sectors used in the magnetic measurements. These data come

from measurements performed during a series of dedicated calibration runs.

Values $\Delta B^n_{i,s,a}$ calculated using equation (A6) represent the change in local field strength measured in each of the sectors along the shaft during the time interval Δt_i. The changes in integrated field strength, $\Delta B d\ell^n_{i,a}$, per aperture during the time interval Δt_i were then computed as the space integral of the $\Delta B^n_{i,s,a}$ contributions from each sector over the magnet length:

$$\Delta \mathrm{B} d\ell^{\mathrm{n}}_{\mathrm{i,a}} = \int_{\substack{\text{magnet}\\ \text{length}}} \Delta \mathrm{B}^{\mathrm{n}}_{\mathrm{i,s,a}}\, \mathrm{d}\ell \qquad \text{(A9)}$$

For the integration of equation (A9) we took into account the exact position and length of each of the sectors as well as the gaps situated among them. We assumed the magnetic field in the gaps to be equal to the average magnetic field measured on the two nearby sectors.

In order to calculate the absolute field strength per magnet aperture we added the initial value of the field, $B^n_{o,a}$, to $\Delta B d\ell^n_{i,a}$. $B^n_{o,a}$ was deduced from rotating coil measurements performed during the magnet characterisation. The absolute field strength per aperture at every time-stamp was then calculated by:

$$\mathrm{B}^{\mathrm{n}}_{\mathrm{i,a}} = \mathrm{B}^{\mathrm{n}}_{\mathrm{o,a}} + \Delta \mathrm{B} d\ell^{\mathrm{n}}_{\mathrm{i,a}} \qquad \text{(A10)}$$

We observed that the quality of our results improved considerably when we fixed the slope of the calculated $B^n_{i,a}$ (n=1,2) field strength versus current to match the slope of the respective curve measured with rotating coils. This technique is equivalent to correcting the calibration factors K_n so as to eliminate errors introduced due to the uncertainty in the extrapolation of the coil geometry to operating conditions, misaligned shafts with respect to the field axis, unquantified effects of read-out electronics and systematic differences among the test bench measurement systems.

In Figure A1 we plot the calculated dipole and quadrupole strengths, B_1 and B_2, for apertures 1 of MB2624 (Figure A1a) and SSS064 (Figure A1b) before and after calibration with rotating coil measurements. We also present the rotating coil field strengths.

Since all power converters were synchronized, we then computed the instantaneous values of the ratios B_2/B_1 and B_1/B_1 by taking the ratio of the numerical values of B_1 and B_2 at each time. We note that problems associated with the raw data files (hardware problems like failures in cable interconnections which led to wrong measured values and errors in data entry of the acquisition system) didn't allow us to compute the B_2/B_1 and B_1/B_1 ratios for all tracking tests performed.

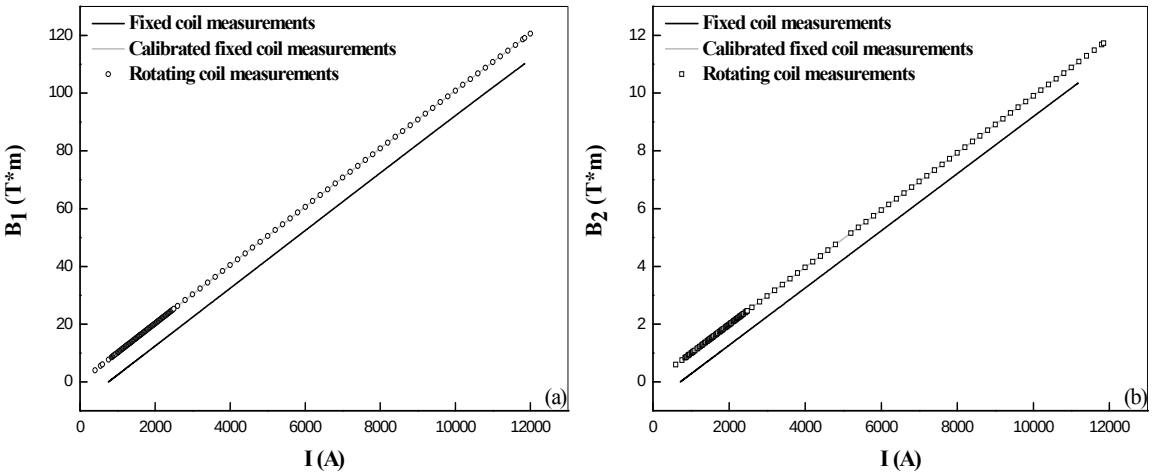

Figure A1: Field strength measured on aperture 1 **(a)** of dipole MB2624 and **(b)** quadrupole SSS064 with fixed and rotating coils. The results of calibration of fixed coil measurements with rotating coil measurements are also presented.

APPENDIX B - CALIBRATION FACTORS

Below we summarize the length, position in the shaft and coil sensitivities for all sectors of shafts used for the magnetic measurements. These data have been measured during series of dedicated calibration runs and have been used for our calculations.

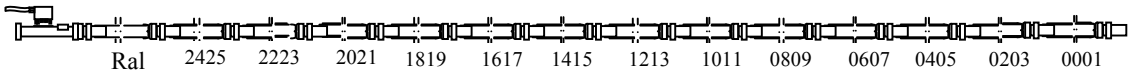

Figure B1: A schematic of the shafts installed in the apertures of the main dipoles for the magnetic measurements.

Table B1: Naming, length, position and calibration factors K_2 for sectors of shaft co-h35 installed in aperture 1 of SSS064. PDIs read added signals from outermost coils A, E.

Sector name	Length (m)	Position (m)	Total K_2 (m^2)
s0203	0.70007	1.18531	0.7551
s0405	0.70007	1.99543	0.7340
s0607	0.70007	2.80653	0.7364
s0809	0.70007	3.61682	0.7393
s1011	0.70007	4.42823	0.7593

Table B2: Naming, length, position and calibration factors K_2 for sectors of shaft co-h36 installed in aperture 2 of SSS064. PDIs read added signals from outermost coils A, E.

Sector name	Length (m)	Position (m)	Total K_2 (m^2)
s0203	0.70007	1.18610	0.7465
s0405	0.70007	1.99731	0.7397
s0607	0.70007	2.80865	0.7389
s0809	0.70007	3.61894	0.7369
s1011	0.70007	4.42908	0.7624

Table B3: Naming, length, position and calibration factors K_1 for sectors of shaft co-h27 installed in aperture 1 of MB2624. PDIs read signal from coil A.

Sector name	Length (m)	Position (m)	K_1 (m^2)
s0001	1.15018	15.779	0.3537
s0203	1.15018	14.519	0.3441
s0405	1.15018	13.259	0.3532
s0607	1.15018	11.999	0.3535
s0809	1.15018	10.739	0.3541
s1011	1.15018	9.479	0.3522
s1213	1.15018	8.219	0.3557
s1415	1.15018	6.959	0.3497
s1617	1.15018	5.699	0.3533
s1819	1.15018	4.439	0.3536
s2021	1.15018	3.179	0.3511
s2223	1.15018	1.919	0.3521

Table B4: Naming, length, position and calibration factors K_1 for sectors of shaft co-h28 installed in aperture 2 of MB2624. PDIs read signal from coil A.

Sector name	Length (m)	Position (m)	K_1 (m^2)
s0001	1.15018	15.779	0.3584
s0203	1.15018	14.519	0.3526
s0405	1.15018	13.259	0.3516
s0607	1.15018	11.999	0.3534
s0809	1.15018	10.739	0.3530
s1011	1.15018	9.479	0.3528
s1213	1.15018	8.219	0.3553
s1415	1.15018	6.959	0.3523
s1617	1.15018	5.699	0.3537
s1819	1.15018	4.439	0.3514
s2021	1.15018	3.179	0.3502
s2223	1.15018	1.919	0.3501

Table B5: Naming, length, position and calibration factors K_1 for sectors of shaft co-h30 installed in aperture 1 of MB2598. PDIs read signal from coil A.

Sector name	Length (m)	Position (m)	K_1 (m^2)
s0001	1.15018	15.779	0.3545
s0203	1.15018	14.519	0.3518
s0405	1.15018	13.259	0.3531
s0607	1.15018	11.999	0.3499
s0809	1.15018	10.739	0.3515
s1011	1.15018	9.479	0.3539
s1213	1.15018	8.219	0.3554
s1415	1.15018	6.959	0.3561
s1617	1.15018	5.699	0.3567
s1819	1.15018	4.439	0.3540
s2021	1.15018	3.179	0.3512
s2223	1.15018	1.919	0.3539

Table B6: Naming, length, position and calibration factors K_1 for sectors of shaft co-h29 installed in aperture 2 of MB2598. PDIs read signal from coil A.

Sector name	Length (m)	Position (m)	K_1 (m^2)
s0001	1.15018	15.779	0.3550
s0203	1.15018	14.519	0.3549
s0405	1.15018	13.259	0.3540
s0607	1.15018	11.999	0.3466
s0809	1.15018	10.739	0.3516
s1011	1.15018	9.479	0.3621
s1213	1.15018	8.219	0.3596
s1415	1.15018	6.959	0.3566
s1617	1.15018	5.699	0.3512
s1819	1.15018	4.439	0.3603
s2021	1.15018	3.179	0.3533
s2223	1.15018	1.919	0.3512

APPENDIX C – ERROR ANALYSIS

The very tight windows for the maximum allowable variation of ratios B_2/B_1 and B_1/B_1 have to be compared with the unavoidable errors introduced in our results by the measurement method.

Measurements of voltage signals during periods of constant current, i.e. at flat bottom and at flat top plateaus showed that the mean value and the rms amplitude vary from coil to coil for both the dipole and the quadrupole, with values within the μV scale. In Figures 8 and 9 the measured mean values and the rms amplitudes of the voltage noise for the 1st LHC cycle performed on Friday 19/10/2007 are shown.

For the calculation of the dipole and quadrupole field strengths the elimination of the noise from the measured voltage signals was necessary. Thus, the noise mean values were removed from each coil signal by means of a linear interpolation with the current, following [10]. However, the method of eliminating the voltage noise from the measured voltage signals, although effective was not completely successful. Below follows an estimation of the uncertainty introduced in our results due to the residual voltage noise which could not be effectively removed from the measured voltage signals and hence was integrated all along with the voltage signals.

The uncertainty in the estimation of the average voltage levels $\Delta V_{off,s,a}$ (standard error on the mean value) is:

$$\delta(\Delta V_{off,s,a}) = \sqrt{\frac{\sum_{i=1}^{N}\left(\Delta V_{i,s,a} - \Delta V_{off,s,a}\right)^2}{N(N-1)}} = \frac{RMS_{s,a}}{\sqrt{N-1}} \quad [\wp] \qquad (C1)$$

where $RMS_{s,a}$ is the root mean square variation of the voltage noise values around their average value $\Delta V_{off,s,a}$. s indicates the numbering of the sectors of the shafts connected to the acquisition system, a indicates the magnet's aperture and i indicates the N measurements taken during a flat-bottom or a flat-top plateau. As in the case of the mean voltage offset, for each LHC cycle, for each aperture and for each sector we compute two $\delta(\Delta V_{off,s,aFB})$ and $\delta(\Delta V_{off,s,aFT})$ uncertainty values, referring to flat-bottom and flat-top plateaus, respectively.

Consequently, the uncertainty in the correction of the measured voltages, i.e. in equation (A3), will be:

$$\delta(\Delta Vcorr_{i,s,a}) = \sqrt{\left((1-\xi)\cdot\delta\left(\Delta V_{off,s,a_{FB}}\right)\right)^2 + \left(\xi\cdot\delta\left(\Delta V_{off,s,a_{FT}}\right)\right)^2} \qquad (C2)$$

where function ξ is already defined in equation (A4). In Figure C1 we plot the uncertainty $\delta(\Delta Vcorr_{i,s,a})$ calculated for aperture 1 of magnets MB2624 and SSS064. The measured data are coming from the 1st LHC cycle performed on Friday 19/10/2007.

We observe that for the main dipole the uncertainty values, $\delta(\Delta Vcorr_{i,s,a})$, span from 1 to 6 μV for the and from 10 to 50 μV for the main quadrupole. The calculated uncertainty exhibits a current dependent behaviour resulting mainly from the current dependent nature of the rms amplitude as well as from the current dependent formula we used to extract noise levels from the

[℘] We use the symbol δ to denote uncertainties and the symbol Δ to denote increments of a measured quantity.

measured voltages.

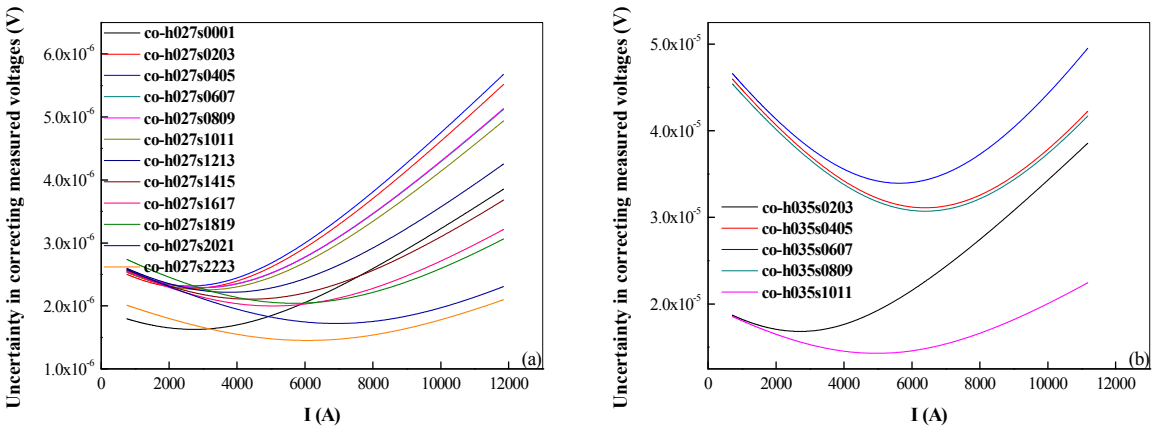

Figure C1: Calculated uncertainty (equation C2) in eliminating noise from measured voltage signals during the 1st LHC cycle performed on Friday 19/10/2007. Uncertainty is calculated for voltage signals measured **(a)** on sectors s0001 through sector s2223 of shaft co-h027 installed in aperture 1 of dipole magnet MB2624 and **(b)** on sectors s0203 through sectors s1011 of shaft co-h35 installed in aperture 1 of quadrupole magnet SSS064.

Then, we performed all calculations explained in Appendix A with the calculated uncertainties $\delta(\Delta Vcorr_{i,s,a})$ instead of the corrected voltage signals, $\Delta Vcorr_{i,s,a}$, in order to get an estimation of the uncertainty in the main field, $B^n_{i,a}$, values. In Figure C2 we quote the calculated uncertainty in B_1 and B_2 values.

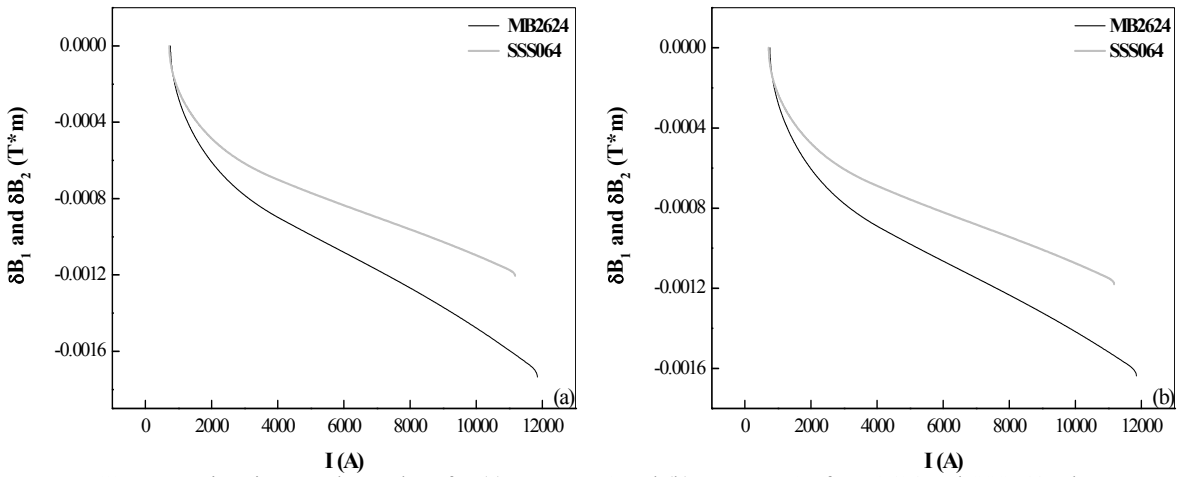

Figure C2: Uncertainty in B_1 and B_2 values for (a) apertures 1 and (b) apertures 2 of MB2624 and SSS064. The zero value of the uncertainty at injection current is justified by the fact that the integration of residual voltage noise starts in the beginning of the ramp-up phase of the cycle at which we set the initial value of the picked-up flux equal to zero.

The statistical uncertainties in B_1 and B_2 field strength values display a current dependent behaviour starting from the zero value at injection current to their maximum value at nominal current. For the main dipole the maximum value of δB_1 at nominal current is around $1.6 \cdot 10^{-3}$ T·m, while for the main quadrupole the maximum value of δB_2 is around $1.2 \cdot 10^{-3}$ T·m (both uncertainty values are given in absolute values). After uncertainties δB_1 and δB_2 are estimated, the overall uncertainty $\delta(B_2/B_1)$, which will be called 'instrumentation error', can be calculated using:

$$\delta\left(\frac{B_2}{B_1}\right)=\sqrt{\left(\frac{\delta B_2}{B_1}\right)^2+\left(\frac{B_2\cdot\delta B_1}{B_1^2}\right)^2} \qquad \text{(C3)}$$

The 'instrumentation error' $\delta(B_2/B_1)$ is not constant but exhibits a complex current dependence stemming from equation (C3) used. It is plotted in Figure C3 for both apertures of MB2624 and SSS064. Its values vary from $1\cdot10^{-6}$ to $2.5\cdot10^{-5}$ leading to an uncertainty of 0.01 to 0.25 units in our results.

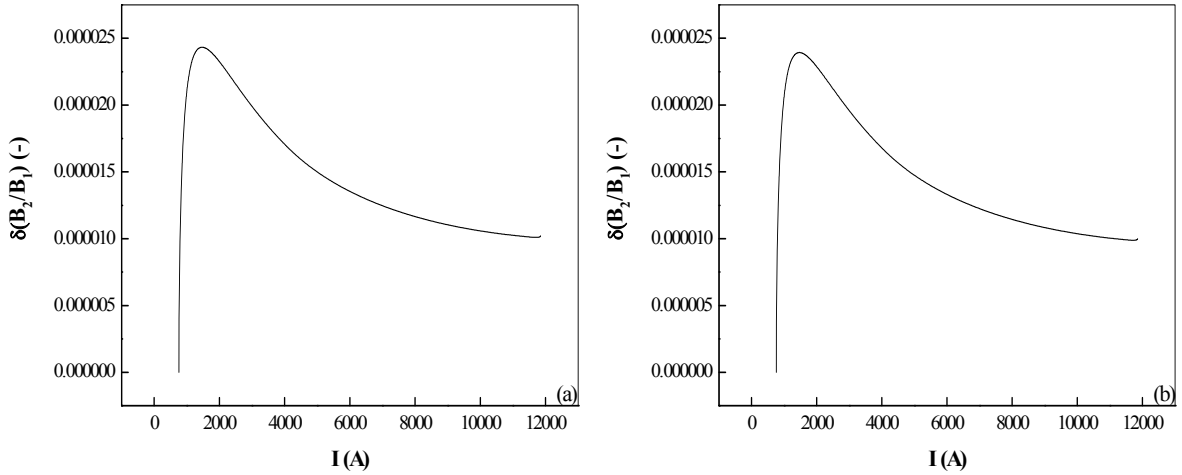

Figure C3: Analysis error $\delta(B_2/B_1)$ for (a) apertures 1 and (b) apertures 2 of MB2624 and SSS064.

The 'instrumentation error' reflects the limitations in the measurement accuracy that can be achieved as well in the compensation of the measurement uncertainties by the chosen analysis method. Finally, we note that the 'instrumentation error' values don't change from cycle to cycle since they depend only on the measurement configuration.

APPENDIX D - VARIATION OF MEASURED CORRECTOR STRENGTH VS COIL POSITION

The variation of the corrector strength as a function of sector position is shown in Figure C1. The variation is considerable and is thought to originate due to the variation of the rotating coil surface along the sector. The red point round about 500mm is where the corrector is originally characterized whilst the red point round about 50mm is the point where the corrector is measured during the compensation measurement. In the case of magnet 2624, the difference between the two points is quite large. In order to eliminate this contribution from the tracking experiment, the correctors were characterised at their b3 compensation position (i.e. the standard magnetic measurement position).

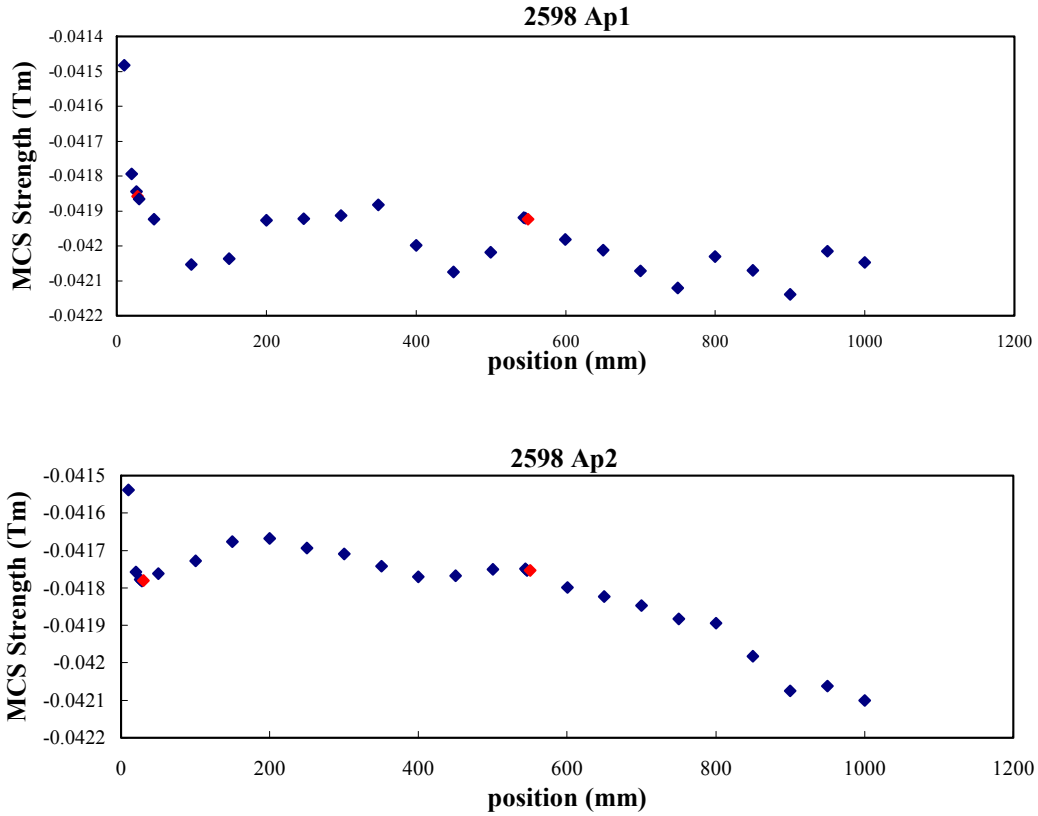

Figure D1: Variation of corrector strength as a function of sector position for magnet 2598 using shafts 30 and 29 for aperture 1 and aperture 2 respectively.

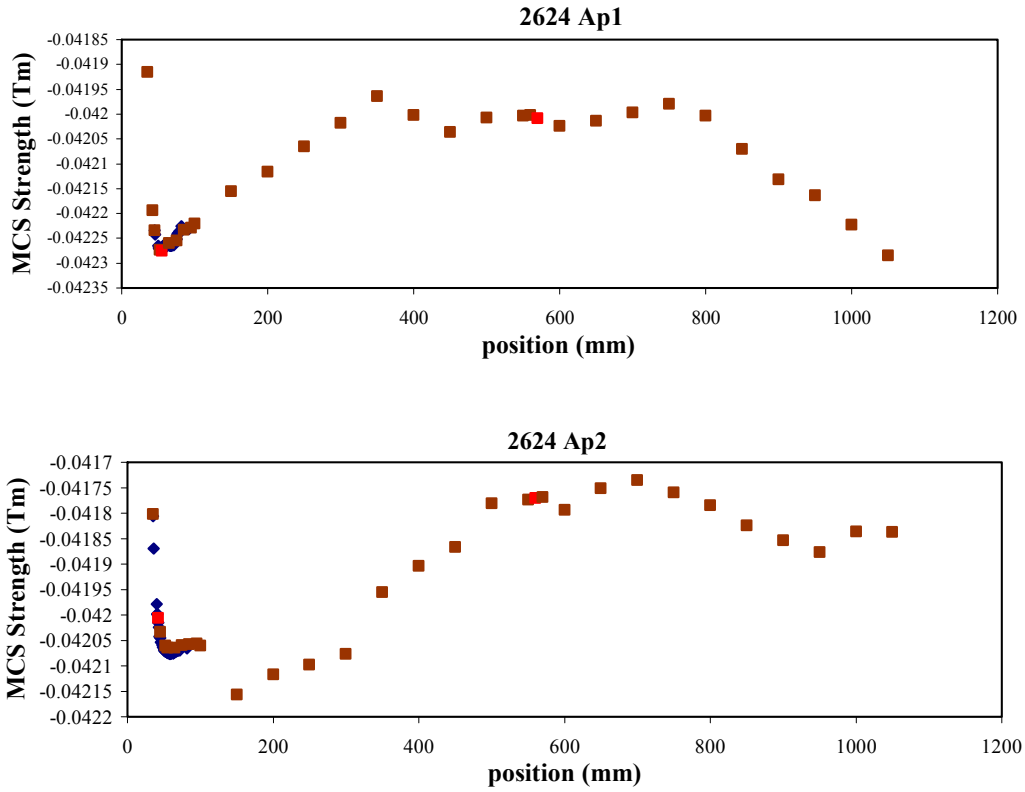

Figure D2: Variation of corrector strength as a function of sector position for magnet 2624 using shafts 27 and 28 for aperture 1 and aperture 2 respectively.

APPENDIX E - DIFFERENCE IN LOADLINE MEASUREMENTS

In order to check the stability of the magnets and the reproducibility of the measurements, two standard loadline measurements were performed on magnet 2624 in aperture 1 using shaft 25. This resulted in a difference of about 0.2 units at injection current. The detailed loadline measurement used to characterise the magnet for the b3 compensation experiment also varied from the other loadlines. The source of this variation is still unknown but it may be the source of the residual sextupole in the compensation experiment.

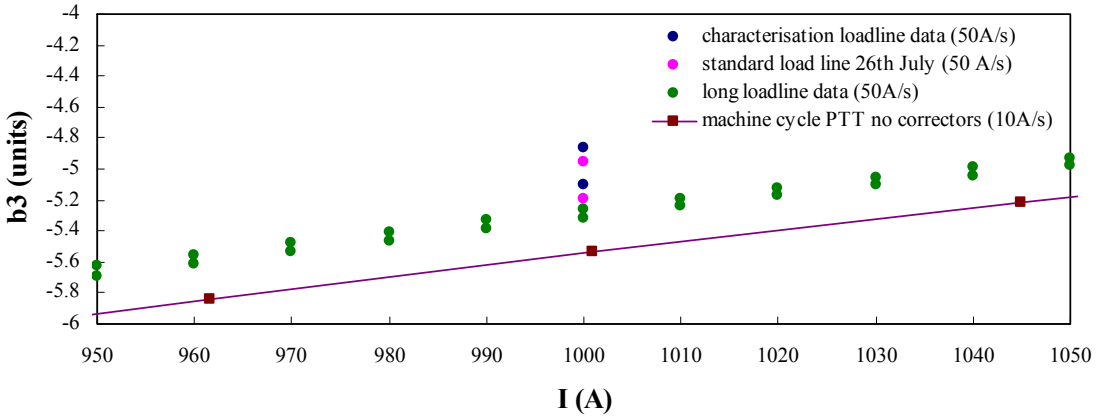

Figure E1: The loadline measurements performed to investigate the stability of the magnet.